

Improving Uncertainty Quantification of Variance Networks by Tree-Structured Learning

Wenxuan MA and Xing YAN

Abstract—To improve uncertainty quantification of variance networks, we propose a novel tree-structured local neural network model that partitions the feature space into multiple regions based on uncertainty heterogeneity. A tree is built upon giving the training data, whose leaf nodes represent different regions where region-specific neural networks are trained to predict both the mean and the variance for quantifying uncertainty. The proposed Uncertainty-Splitting Neural Regression Tree (USNRT) employs novel splitting criteria. At each node, a neural network is trained on the full data first, and a statistical test for the residuals is conducted to find the best split, corresponding to the two sub-regions with the most significant uncertainty heterogeneity. USNRT is computationally friendly because very few leaf nodes are sufficient and pruning is unnecessary. On extensive UCI datasets, in terms of both calibration and sharpness, USNRT shows superior performance compared to some recent popular methods for variance prediction, including vanilla variance network, deep ensemble, dropout-based methods, tree-based models, etc. Through comprehensive visualization and analysis, we uncover how USNRT works and show its merits.

Index Terms—Variance Networks, Uncertainty Heterogeneity, Tree-Structured Learning, Statistical Test

I. INTRODUCTION

Deep learning has achieved great successes in many fields or applications, such as computer vision, natural language processing, protein structure prediction, and game playing [1]. The most attractive feature of deep learning is the remarkable prediction accuracy it can obtain. However, there are still serious concerns preventing deep learning from deploying extensively in real life, including their opacity in making predictions, their fragility in facing diverse inputs, and their over-confidence in the prediction results. Especially in risk-sensitive decision-makings, practitioners do not allow certain types of errors made by machines. Uncertainty quantification aims to alleviate those concerns partly by giving a confidence accompanied with each prediction result. Good uncertainty estimation can avoid over-confidence [2], [3] and reduce the risk of making unacceptable errors for decision-makers. Therefore, it is worthwhile to make efforts to produce good uncertainty estimation and only trust outcomes with high confidence.

There are several types of uncertainty quantification methods for neural networks proposed recently. Bayesian methods [4]–[8] use the estimated posterior density function to quantify uncertainty. Generally, approximation computation is needed

to overcome the computational issue. With Gaussian distribution assumption, some works [9]–[12] use neural network models to produce two outputs, the mean and the variance, for quantifying uncertainty. Quantile regression-based models [13]–[15] quantify uncertainty by estimating a group of conditional quantiles, to further form prediction intervals. In this paper, we focus on the mean and variance prediction and aim to improve uncertainty quantification of the variance networks.

A key observation made by us is that data exhibits uncertainty heterogeneity across different regions in the feature space, as illustrated in Figure 3 and 4 in the experimental section. Thereby, discovering heterogeneity via partitioning the space is motivated. With the emergence of complex, diverse, and large-scale datasets, reducing the difficulty of modeling through space partitioning or data partitioning becomes necessary, making machine learning tasks (uncertainty quantification tasks in this paper) less challenging. In the past, some researchers used data partitioning as a pre-method [16], [17] and sub-model was fitted within each region. Some region-specific models [18]–[20] and tree-based models [21], [22] were proposed with similar goals. As far as we know, there were very few works tackling the challenging uncertainty quantification tasks of deep learning with data heterogeneity and data partitioning considerations.

In this paper, we propose a novel tree-based neural network model called Uncertainty-Splitting Neural Regression Tree (USNRT) which partitions the feature space recursively based on novel splitting criteria for discovering uncertainty heterogeneity. It gives the prediction and uncertainty estimation based on region-specific sub-models. For the splitting criteria, a neural network is trained first at each internal node and a statistical test is conducted on the residuals to help assess the uncertainty heterogeneity between the two sub-regions. In each leaf region, two region-specific neural networks are used to predict the mean and the variance respectively. Intuitively, this can reduce the difficulty of modeling compared to the full-space modeling approach.

The proposed USNRT has a computational complexity proportional to the tree depth, and pruning is unnecessary. As we can see in the experimental section, generally, a tree with depth 2, 3, or at most 4 is enough to produce good performance. Thus, USNRT’s computational cost is satisfactory. We apply it on 17 extensive UCI datasets of various sizes and compare it with existing representative methods. The experimental results show that USNRT achieves superior performance over others. Furthermore, comprehensive visualization and analysis indi-

Both the authors are with the Institute of Statistics and Big Data, Renmin University of China (e-mail: {mawenxuan,xingyan}@ruc.edu.cn).

Corresponding author: Xing YAN.

cate that such a tree-structured learning method is successful and interpretable, and has merits as stated.

Code and data for reproducing all the experimental results are available in the link¹.

II. RELATED WORKS

We review the related works of both variance prediction and tree-based space partitioning. We aim for their combination.

A. Variance Networks and Uncertainty Quantification

HNN and Deep Ensemble. Given the feature vector, the conditional distribution of the continuous label is assumed to be Gaussian. Variance network methods try to output its mean and variance. However, their training is not straightforward. There were some works proposing various training schemes. For instance, [9] used one network to output both the mean and the variance, and adopted the negative log-likelihood loss and a gradient clipping strategy. [11] combined the negative log-likelihood loss with a new mPAIC loss and trained randomized regression functions to achieve individual calibration. [10] proposed a new mini-batching scheme and trained a mean network and a variance network separately and alternately. These methods are collectively named by us as Heteroscedastic Neural Networks (HNNs). Furthermore, multiple means and variances given by several HNNs with different random initializations can be aggregated to form a final mean and a final variance, which is called the Deep Ensemble method [9].

Dropout-based Bayesian methods. The Bayesian approach has tried early to estimate the mean and variance. Bayesian methods first give the network's parameters a prior distribution, and then given the training data, they compute the posterior distribution of the parameters and the label, which can be further used to quantify uncertainty. However, these methods have a prohibitive computational cost. Various Bayesian approximations were developed to overcome the computational issue. [5] made use of the expectation propagation to estimate the posterior distribution by a set of local approximations. MC Dropout [6] and Concrete Dropout [7] used dropout as a Bayesian approximation. They can estimate the mean and variance and are much simpler to implement.

Tree models with variance estimation. On structured data, it is common to use ensemble tree models to achieve good prediction accuracy. Because our methodology is related to tree models, we should focus on those which can estimate the variance as the uncertainty measurement. Random Forest [23] is a famous ensemble tree model and can return the standard deviation accompanied with the prediction value. Extremely Randomized Tree (ExTra) [24] is another popular ensemble tree model which randomly selects the split points and then chooses the best split. ExTra can return the standard deviation (possibly larger than that given by Random Forest) with the prediction value too. There are some other differences between Random Forest and ExTra. We will use both of them to obtain the mean and variance for quantifying uncertainty.

B. Space Partitioning and Tree Models

Space partitioning is inherent in tree models, where linear and hard (compared to soft) partitioning is adopted. Many tree-based models have been proposed, most of which recursively partition the feature space in an axis-parallel way. Most notably, CART [25] constructs the tree structure by greedily partitioning the data to decrease the sum of squared errors and uses constant-valued models within nodes. In recent years, some studies have contributed to upgrading the predictive performance of tree models and reducing computation costs. For example, [21] proposed piecewise polynomial regression tree (SUPPORT) which recursively utilizes the estimated residuals' signs to divide data into two parts. It determines the best split by conducting a statistical test. Finally, node-specific polynomial models were fitted within leaf nodes. Segmented linear regression tree (SLRT) [22] fits a linear model at each node and calculate the cumulative Kendall's τ rank correlation between covariates and estimated residuals to select the best partition. Piecewise polynomial or linear tree models are useful, but may not be attractive given the complexity, nonlinearity, and heterogeneity of large real-world datasets. When deep learning is extremely popular and has excellent expressive power, as far as we know, there were very few works that combine the tree models with neural networks such that node-specific networks are employed for leaf nodes.

III. THEORETICAL JUSTIFICATION

We first justify the usefulness of space partitioning theoretically. We show that if the data-generating process is heterogeneous, partitioning the feature space always yields a smaller expected risk.

Proposition 1: Suppose two uncountable infinite sets $\mathcal{D}_0 \cup \mathcal{D}_1 = \mathbb{R}^d$, $\mathcal{D}_0 \cap \mathcal{D}_1 = \emptyset$, and the closures $\overline{\mathcal{D}_0} \cap \overline{\mathcal{D}_1} = \{x \in \mathbb{R}^d | B(x) = 0\} \neq \emptyset$, where $B(\cdot) \in C^0(\mathbb{R}^d)$. Assume $\mathbf{y}_0 = f_0(\mathbf{X}_0) + \varepsilon_0$, $\mathbf{y}_1 = f_1(\mathbf{X}_1) + \varepsilon_1$, where $f_0 \in C^0(\overline{\mathcal{D}_0})$, $f_1 \in C^0(\overline{\mathcal{D}_1})$, and $\mathbf{X}_0, \mathbf{X}_1, \varepsilon_0, \varepsilon_1$ are mutually independent random variables: $\mathbf{X}_0 : \Omega \rightarrow \mathcal{D}_0$, $\mathbf{X}_1 : \Omega \rightarrow \mathcal{D}_1$, and $\varepsilon_0, \varepsilon_1$ are noise variables with constant parameters. If another independent $Z \sim \text{Bernoulli}(p)$, let $\mathbf{X} = Z\mathbf{X}_1 + (1 - Z)\mathbf{X}_0$ and $\mathbf{y} = Z\mathbf{y}_1 + (1 - Z)\mathbf{y}_0$, given a proper loss function l (such as least square), we have

$$\begin{aligned} & (1 - p) \min_{f \in \mathcal{F}} \mathbb{E} [l(\mathbf{y}_0, f(\mathbf{X}_0))] + p \min_{f \in \mathcal{F}} \mathbb{E} [l(\mathbf{y}_1, f(\mathbf{X}_1))] \\ & \leq \min_{f \in \mathcal{F}} \mathbb{E} [l(\mathbf{y}, f(\mathbf{X}))], \end{aligned} \quad (1)$$

where \mathcal{F} is a function set (such as neural networks) satisfying $\mathcal{F} \subset C^0(\mathbb{R}^d)$.

Proof: According to the double expectation formula, we have

$$\begin{aligned} & \mathbb{E} [l(\mathbf{y}, f(\mathbf{X}))] \\ & = \mathbb{E} [l(Z\mathbf{y}_1 + (1 - Z)\mathbf{y}_0, f(Z\mathbf{X}_1 + (1 - Z)\mathbf{X}_0))] \\ & = \mathbb{E} [\mathbb{E} [l(Z\mathbf{y}_1 + (1 - Z)\mathbf{y}_0, f(Z\mathbf{X}_1 + (1 - Z)\mathbf{X}_0)) | Z]] \\ & = (1 - p) \mathbb{E} [l(\mathbf{y}_0, f(\mathbf{X}_0))] + p \mathbb{E} [l(\mathbf{y}_1, f(\mathbf{X}_1))] \\ & \geq (1 - p) \min_{f \in \mathcal{F}} \mathbb{E} [l(\mathbf{y}_0, f(\mathbf{X}_0))] + p \min_{f \in \mathcal{F}} \mathbb{E} [l(\mathbf{y}_1, f(\mathbf{X}_1))]. \end{aligned}$$

Therefore, if we take the minimum of $\mathbb{E} [l(\mathbf{y}, f(\mathbf{X}))]$ for $f \in \mathcal{F}$, we can finish the proof. \blacksquare

¹<https://github.com/xingyan-fml/usnrt>

Corollary 2: Under the conditions of Proposition 1, we consider the heteroscedasticity situation. Now we assume $\mathbf{y}_0 = f_0(\mathbf{X}_0) + \sigma_0(\mathbf{X}_0)\varepsilon_0$ and $\mathbf{y}_1 = f_1(\mathbf{X}_1) + \sigma_1(\mathbf{X}_1)\varepsilon_1$, where $\sigma_0 \in C^0(\overline{\mathcal{D}_0})$, $\sigma_1 \in C^0(\overline{\mathcal{D}_1})$, given a proper loss function $l(\cdot, \cdot, \cdot)$ between y and $(f(x), \sigma(x))$ (such as negative log-likelihood), we have

$$\begin{aligned} & (1-p) \min_{f \in \mathcal{F}, \sigma \in \mathcal{F}'} \mathbb{E}[l(\mathbf{y}_0, f(\mathbf{X}_0), \sigma(\mathbf{X}_0))] \\ & + p \min_{f \in \mathcal{F}, \sigma \in \mathcal{F}'} \mathbb{E}[l(\mathbf{y}_1, f(\mathbf{X}_1), \sigma(\mathbf{X}_1))] \\ & \leq \min_{f \in \mathcal{F}, \sigma \in \mathcal{F}'} \mathbb{E}[l(\mathbf{y}, f(\mathbf{X}), \sigma(\mathbf{X}))], \end{aligned} \quad (2)$$

where \mathcal{F} and \mathcal{F}' are function sets satisfying $\mathcal{F} \subset C^0(\mathbb{R}^d)$, $\mathcal{F}' \subset C^0(\mathbb{R}^d)$. ■

Proposition 3: Under the conditions of Corollary 2, the inequality in Corollary 2 is strict if we further assume the following conditions are satisfied:

- 1) \mathbf{X}_0 and \mathbf{X}_1 have positive densities over \mathcal{D}_0 and \mathcal{D}_1 respectively;
- 2) either f_0, f_1 or σ_0, σ_1 are discontinuous at some points on the boundary between \mathcal{D}_0 and \mathcal{D}_1 ;
- 3) \mathcal{F} is closed under addition, and the functions composed by $Wx + b$ and $\max(x, 0)$ with at most T_{max} times and d_{max} internal dimensions, are in \mathcal{F} . $f \in \mathcal{F}'$ if $f \in \mathcal{F}$ and $f > 0$. $T \circ f \in \mathcal{F}'$ if $f \in \mathcal{F}$ and $T \in C^0(\mathbb{R})$, $T > 0$.

The similar conclusion applies on the inequality in Proposition 1 too. Moreover, the conclusion applies for other activation functions beyond $\max(x, 0)$, such as Sigmoid and Tanh.

Proof Sketch: Without loss of generality, we assume f_0 and f_1 are discontinuous at the point x^* on the boundary between \mathcal{D}_0 and \mathcal{D}_1 . Suppose $\min_{f \in \mathcal{F}, \sigma \in \mathcal{F}'} \mathbb{E}[l(\mathbf{y}, f(\mathbf{X}), \sigma(\mathbf{X}))]$ is solved at f^*, σ^* , because f^* is a continuous function and f_0, f_1 are continuous on $\overline{\mathcal{D}_0}$ and $\overline{\mathcal{D}_1}$ respectively, we can find a hypercube H centered at x^* with length δ such that:

$$\begin{aligned} |f^*(x) - f^*(x^*)| &< \epsilon/8, \quad x \in H, \\ |f_0(x) - f_0(x^*)| &< \epsilon/8, \quad x \in H \cap \mathcal{D}_0, \\ |f_1(x) - f_1(x^*)| &< \epsilon/8, \quad x \in H \cap \mathcal{D}_1, \end{aligned}$$

where $\epsilon = |f_1(x^*) - f_0(x^*)|$. This can easily yield $|f^*(x) - f_0(x)| > \epsilon/4$ for all $x \in H \cap \mathcal{D}_0$, or, $|f^*(x) - f_1(x)| > \epsilon/4$ for all $x \in H \cap \mathcal{D}_1$. Without loss of generality, we assume the former is true, then we can further find an $f_2 \in \mathcal{F}$ according to the condition 3), such that $f_2(x) = 0$ when $x \notin H$, and $f^* + f_2$ gives:

$$\begin{aligned} & \mathbb{E}[l(\mathbf{y}_0, (f^* + f_2)(\mathbf{X}_0), \sigma^*(\mathbf{X}_0))] \\ & < \mathbb{E}[l(\mathbf{y}_0, f^*(\mathbf{X}_0), \sigma^*(\mathbf{X}_0))]. \end{aligned}$$

This inequality holds because \mathbf{X}_0 and \mathbf{X}_1 have positive densities around x^* and l is a proper loss such that a better $f \in \mathcal{F}$ will lead to a smaller expected risk. With this inequality, we can finish the proof. The full proof is in Appendix A. ■

IV. METHODOLOGY

In this section, we describe how to construct the proposed Uncertainty-Splitting Neural Regression Tree (USNRT). The algorithm details are also included in Algorithm 1.

A. Framework

We focus on the regular regression problem between the outcome \mathbf{y} and the features $\mathbf{X} = (\mathbf{X}_1, \dots, \mathbf{X}_d)^\top$, given the dataset $\{(\mathbf{X}(i), \mathbf{y}(i))\}_{i=1}^N$, where $\mathbf{X}(i) \in \mathcal{X}$ and \mathcal{X} is the feature space. We hope to build a model that captures the heterogeneity across M disjoint regions $\{\mathcal{R}_m\}_{m=1}^M$ partitioned from \mathcal{X} , satisfying $\mathcal{X} = \bigcup_{m=1}^M \mathcal{R}_m$. For different regions, the prediction models and the uncertainty estimation models are distinct. To be formal, our model is

$$\mathbf{y} = \sum_{m=1}^M (f_m(\mathbf{X}) + \sigma_m(\mathbf{X})\varepsilon_m) \mathbb{I}_{\{\mathbf{X} \in \mathcal{R}_m\}}, \quad (3)$$

where $f_m(\mathbf{X})$ predicts \mathbf{y} given \mathbf{X} locating in the region \mathcal{R}_m , and $\sigma_m(\mathbf{X})$ denotes the individual uncertainty level. We assume ε_m is standard Gaussian-distributed.

We further assume that the regions $\{\mathcal{R}_m\}_{m=1}^M$ are obtained by recursively partitioning \mathcal{X} in an axis-parallel way. In the context of tree models, that is, at each internal node t , we choose both the best split variable $\mathbf{X}_{\hat{k}}$ and the best split value \hat{a} under some splitting criteria to obtain two child nodes: $\mathbf{X}_{\hat{k}} \leq \hat{a}$ and $\mathbf{X}_{\hat{k}} > \hat{a}$.

B. Recursive Partitioning with Uncertainty Heterogeneity

When constructing the tree with training data, at each internal node t , we first train a neural network model $\hat{f}_{\text{split}}(\mathbf{X})$ with the data in the node using the mean squared error loss. Then we can obtain the residual $\hat{\mathbf{e}} = \mathbf{y} - \hat{f}_{\text{split}}(\mathbf{X})$.

If the region of node t is partitioned into two sub-regions, we want to check whether the overall uncertainty levels in this two sub-regions are heterogeneous. If yes, the node t will be divided to reduce the difficulty of modeling. To measure the overall uncertainty level, we use the sample variance of the residual $\hat{\mathbf{e}}$. Therefore, our goal is simplified to verifying whether we can partition the residuals $\{\hat{\mathbf{e}}(i)\}$ into two groups, such that the residuals' variances in the two groups are significantly different. We can conduct such an examination with the help of Levene's test [26], which is a statistical tool to test the equality of variances of two groups of observations.

For an arbitrary split choice with split variable \mathbf{X}_k and split value a , there will be two separate index sets of the data samples: $\mathcal{I}_L = \{i | \mathbf{X}_k(i) \leq a\}$ and $\mathcal{I}_R = \{i | \mathbf{X}_k(i) > a\}$. Correspondingly, we can obtain two groups of residuals: $\hat{\mathbf{e}}_L = \{\hat{\mathbf{e}}(i) | i \in \mathcal{I}_L\}$ and $\hat{\mathbf{e}}_R = \{\hat{\mathbf{e}}(i) | i \in \mathcal{I}_R\}$. Let \bar{e}_* and $\hat{\sigma}_*^2$ denote the sample mean and sample variance of $\hat{\mathbf{e}}_*$, where $*$ represents the subscript L or R . In Levene's test [26], the null hypothesis is the equality of the two variances:

$$H_0: \sigma_L^2 = \sigma_R^2. \quad (4)$$

We define $\mathbf{z}_* = \{|\hat{\mathbf{e}}(i) - \bar{e}_*| | i \in \mathcal{I}_*\}$, and let \bar{z}_* and w_*^2 denote the sample mean and sample variance of \mathbf{z}_* . Then the pooled variance is defined as $w_{\text{pool}}^2 = \frac{(|\mathcal{I}_L|-1)w_L^2 + (|\mathcal{I}_R|-1)w_R^2}{|\mathcal{I}_L| + |\mathcal{I}_R| - 2}$. Following [21], the Levene's test statistic is defined as follows:

$$T_{\text{Levene}} = \frac{\bar{z}_L - \bar{z}_R}{w_{\text{pool}} \sqrt{|\mathcal{I}_L|^{-1} + |\mathcal{I}_R|^{-1}}}. \quad (5)$$

This test statistic follows a Student's t -distribution with $|\mathcal{I}_L| + |\mathcal{I}_R| - 2$ degrees of freedom if the null hypothesis

is supported. We can compute the corresponding p -value, denoted as $p(k, a)$, for each split choice \mathbf{X}_k and a . Among all these p -values obtained, we choose the variable index \hat{k} and the split value \hat{a} corresponding to the smallest one as our best split choice:

$$p_{\text{best}} = p(\hat{k}, \hat{a}) = \min_{k, a} p(k, a). \quad (6)$$

If p_{best} is less than a given significance level α , we can reject the null hypothesis of equal variances under this best split choice. Then, we partition the region into two sub-regions: $\mathbf{X}_{\hat{k}} \leq \hat{a}$ and $\mathbf{X}_{\hat{k}} > \hat{a}$, in which the residuals' variances are the most significantly different. So, this node is divided and the data samples in the node are divided into two parts correspondingly. Recursively doing this, we can build a tree.

Our splitting criteria is a little like that of SUPPORT [21] because both use statistical tests. However, SUPPORT only uses the signs of estimated residuals which are much less informative. Instead, our method utilizes the estimated residuals in a more data-driven way and is more intuitive.

C. Stopping Rules

We set two stopping rules to determine whether to divide the node, or to stop and return the current node as a leaf node. First, we ensure that in every node there must be at least N_{min} samples in the tree building. Hence, in the split selection, the split value a should satisfy some constraints to ensure this. Moreover, it helps stop the tree growth. When a node has a sample size less than $2N_{\text{min}}$, it will not be divided anymore. The second stopping rule is that p_{best} obtained from Levene's test should be no more than the given significance level α , otherwise, the current node will not be divided.

The obtained tree can benefit from these two stopping rules. Most importantly, unlike in traditional tree models, pruning is unnecessary for USNRT. In traditional tree models like CART, the splitting criteria is minimizing the sum of square errors in the two child nodes. The deeper the tree is, the more leaf nodes there are, and the more accurate the performance on training data is. Thus, there is a need to balance the accuracy and the complexity of the tree to overcome over-fitting and achieve good generalization. However, our splitting goal is to discover heterogeneity across regions and reduce the difficulty of modeling the data in child nodes. At every leaf node, neural networks will be trained using the data in that node only. Actually, the stopping rules let the tree grow adaptively without the risk of being too shallow or too deep, making the pruning unnecessary. As we will see in the experiments, 10 leaf nodes for USNRT are enough for producing good performance. A consequent benefit is that USNRT will not be computationally costly. The summary of the tree construction is in Algorithm 1.

D. Prediction and Uncertainty Estimation

The prediction and uncertainty estimation are made in every leaf region \mathcal{R}_m separately. When $\mathbf{X} \in \mathcal{R}_m$, two neural networks $f_m(\mathbf{X})$ and $\hat{\sigma}_m(\mathbf{X})$ are used to give the prediction and uncertainty estimation of y . They are trained using the data

Algorithm 1 Uncertainty-Splitting Neural Regression Tree Construction

Require: Dataset $\{(\mathbf{X}(i), y(i))\}_{i=1}^N$, significance level α , minimum sample size of leaf nodes N_{min} , and hyper-parameters of the splitting neural network.

Ensure: A grown tree which partitions the feature space to $\mathcal{X} = \bigcup_{m=1}^M \mathcal{R}_m$, where \mathcal{R}_m is the region of the m -th leaf node.

- 1: Initialize: $m = 0$.
 - 2: Denote the current node as t , and the index set of all samples at this node as \mathcal{I}_t .
 - 3: **if** $|\mathcal{I}_t| < 2N_{\text{min}}$ **then**
 - 4: $m = m + 1$, denote the region of this node as \mathcal{R}_m , and return as a leaf node.
 - 5: **else**
 - 6: Fit a splitting neural network $\hat{f}_{\text{split}}(\mathbf{X})$ with MSE loss using samples in node t , and get the residuals $\hat{e}(i) = y(i) - \hat{f}_{\text{split}}(\mathbf{X}(i))$, $i \in \mathcal{I}_t$.
 - 7: **for** $k = 1$ to d **do**
 - 8: **for** a in sorted $\{\mathbf{X}_k(i) \mid i \in \mathcal{I}_t\}$ **do**
 - 9: Divide the index set into $\mathcal{I}_L = \{i \in \mathcal{I}_t \mid \mathbf{X}_k(i) \leq a\}$ and $\mathcal{I}_R = \{i \in \mathcal{I}_t \mid \mathbf{X}_k(i) > a\}$.
 - 10: **if** $|\mathcal{I}_L| < N_{\text{min}}$ or $|\mathcal{I}_R| < N_{\text{min}}$ **then continue**
 - 11: Divide the residuals into $\hat{e}_L = \{\hat{e}(i) \mid i \in \mathcal{I}_L\}$ and $\hat{e}_R = \{\hat{e}(i) \mid i \in \mathcal{I}_R\}$.
 - 12: Do the Levene's test for the variances of \hat{e}_L and \hat{e}_R and compute the p -value, $p(k, a)$.
 - 13: **end for**
 - 14: **end for**
 - 15: Get $p_{\text{best}} = p(\hat{k}, \hat{a}) = \min_{k, a} p(k, a)$.
 - 16: **if** $p_{\text{best}} > \alpha$ **then**
 - 17: $m = m + 1$, denote the region of this node as \mathcal{R}_m , and return as a leaf node.
 - 18: **else**
 - 19: Split the node t into two child nodes t_L and t_R , where $\mathcal{I}_{t_L} = \{i \in \mathcal{I}_t \mid \mathbf{X}_{\hat{k}}(i) \leq \hat{a}\}$ and $\mathcal{I}_{t_R} = \{i \in \mathcal{I}_t \mid \mathbf{X}_{\hat{k}}(i) > \hat{a}\}$.
 - 20: Let $t = t_L$ and repeat Step 2 – 23.
 - 21: Let $t = t_R$ and repeat Step 2 – 23.
 - 22: **end if**
 - 23: **end if**
-

in \mathcal{R}_m only. Their network structure can be less complicated than that of the splitting neural network used in the internal nodes \hat{f}_{split} . It will be less difficult to model the data in leaf nodes than in internal nodes since the former may not exhibit heterogeneity. Besides, to avoid overfitting, we adopt necessary regularization strategies such as early stopping in all neural network training.

For different leaf regions, we adopt the same training scheme. Different from some recent suggestions on how to train $\hat{f}_m(\mathbf{X})$ and $\hat{\sigma}_m(\mathbf{X})$, we take much simpler training steps. First, $\hat{f}_m(\mathbf{X})$ is trained as usual with the mean square error loss. Then $\hat{f}_m(\mathbf{X})$ is fixed and $\hat{\sigma}_m(\mathbf{X})$ is trained with the negative log-likelihood of Gaussian whose mean and variance

are $\hat{f}_m(\mathbf{X})$ and $\hat{\sigma}_m^2(\mathbf{X})$:

$$\min_{\Theta_m} \sum_{\mathbf{X}(i) \in \mathcal{R}_m} -\log \mathbb{P}(\mathbf{y}(i) | \mathbf{X}(i)) = \sum_{\mathbf{X}(i) \in \mathcal{R}_m} \frac{\log \hat{\sigma}_m^2(\mathbf{X}(i))}{2} + \frac{(\mathbf{y}(i) - \hat{f}_m(\mathbf{X}(i)))^2}{2\hat{\sigma}_m^2(\mathbf{X}(i))} + \text{constant}, \quad (7)$$

where Θ_m is the learnable parameters of $\hat{\sigma}_m(\mathbf{X})$. Some works suggest to train $\hat{f}_m(\mathbf{X})$ and $\hat{\sigma}_m(\mathbf{X})$ simultaneously with a gradient clipping strategy [9], or to train one of them with another fixed alternately and iteratively [10]. The reason why we adopt a simpler training scheme is again that the data in leaf regions may not exhibit heterogeneity and will be less difficult to model. Moreover, this will reduce the computational cost significantly. Finally, USNRT’s prediction and uncertainty estimation are $\hat{f}(\mathbf{X}) = \sum_{m=1}^M \hat{f}_m(\mathbf{X}) \mathbb{I}_{\{\mathbf{X} \in \mathcal{R}_m\}}$ and $\hat{\sigma}(\mathbf{X}) = \sum_{m=1}^M \hat{\sigma}_m(\mathbf{X}) \mathbb{I}_{\{\mathbf{X} \in \mathcal{R}_m\}}$.

To further illustrate the necessity of doing so, we will compute the leaf region-specific residuals’ variance using all $(\mathbf{y}(i) - \hat{f}_m(\mathbf{X}(i)))^2$ when $\mathbf{X}(i) \in \mathcal{R}_m$. In Figure 4 in the experimental section, we show that the variances obtained are quite different or heterogeneous across leaf regions, implying the difficulty of quantifying uncertainty using one model for the whole feature space.

E. Computational Complexity

In tree construction, the two most time-consuming parts are searching for the best splits and training neural networks. The cost of training neural networks depends on the architecture. We use $O(\text{end} \times c(r))$ to denote this cost. Here e is the number of epochs, n is the sample size in a node, d is the feature dimension, r represents the architecture, and c is a function of r . Now the most crucial thing is that as the tree grows to be deeper, we need to train more neural networks. The number of neural networks increases exponentially, but meanwhile, the sample size in the node decreases exponentially. Consequently, the computational cost at every level of the tree remains the same. So, the total computational cost is proportional to the tree depth: $O(hNd \times c(r))$, where h is the tree depth and N is the total sample size. In the experiments, 10 leaf nodes are enough for producing good performance, implying $h \approx 3$. On some datasets, $h \approx 2$ if the total sample size is not large.

The searching for the best split takes $O(dn^2)$ computational cost because we perform Levene’s test $O(dn)$ times. This can be reduced to $O(dn/s)$ times if we set a step size s in searching for the split value a . The cost now is $O(dn^2/s)$ with a very small constant in this O . Furthermore, the cost at every level of the tree will decrease exponentially because of the n^2 term. In our experiments, this part costs much less than training neural networks does and can be ignored.

V. EXPERIMENTS

In this section, we evaluate USNRT and conduct the comparisons to the competing methods comprehensively. We also visualize and interpret the learning results of our method, analyze its stability, and so on.

TABLE I: Dataset information.

Dataset Name	Full Name	Sample Size	Feature Dimension	Categorical Variables
Electrical	Electrical Grid Stability	10,000	12	0
Conditional	Conditional Based Maintenance	11,933	15	0
Appliances	Appliances Energy Prediction	19,735	27	0
Real-time	Real-time Election	21,643	23	0
Industry	Industry Energy Consumption	35,040	9	3
Facebook1	Facebook Comment Volume 1	40,949	52	0
Beijing	Beijing PM2.5	41,757	8	2
Physicochemical	Physicochemical Properties	45,730	9	0
Traffic	Traffic Volume	48,204	6	2
Blog	Blog Feedback	52,397	276	0
Power	Power Consumption of T	52,416	5	0
Online	Online Video	68,784	18	2
Facebook2	Facebook Comment Volume 2	81,312	52	0
Year	Year Prediction MSD	100,000	90	0
Query	Query Analytics	199,843	4	0
GPU	GPU Kernel Performance	241,600	14	4
Wave	Wave Energy Converters	287,999	48	0

A. Data and Settings

Datasets. We collect 17 datasets of regression tasks from the UCI Machine Learning Repository [27]. The sample sizes range from 10,000 to 287,999, and the feature dimensions range from 4 to 276. In some datasets, the categorical variables are also included. For every dataset, we have a short name and a full name. The information of these datasets is detailed in Table I.

Evaluation Settings. For each dataset, we randomly select 80% of the data for training and the rest for testing. With different randomness seeds, this splitting is done five times if the sample size is less than 100,000 and 1 time otherwise (the last four datasets in Table I, for reducing computational burden). For every method, the evaluation metrics are averaged over these training/testing splits. During the training of all neural network models, we choose 20% from the training set as the validation set for early stopping, set the batch size to 64, set the maximum number of epochs to 1,000, and optimize using Adam [28] with the learning rate 0.01. All continuous variables and the label are normalized to have sample mean 0 and sample variance 1. Categorical variables are converted to one-hot encodings.

Structure of USNRT. We denote the feature dimension before one-hot encoding as d . In USNRT, the splitting model $\hat{f}_{\text{split}}(\mathbf{X})$ in the internal nodes is set to have two hidden layers with sizes $[8d, 4d]$. The prediction model $\hat{f}_m(\mathbf{X})$ and uncertainty estimation model $\hat{\sigma}_m(\mathbf{X})$ in the leaf nodes have two hidden layers too, with layer sizes $[4d, 2d]$. For all hidden layers, Tanh activation function is used. All the output layers are linear, except that Softplus is applied in $\hat{\sigma}_m(\mathbf{X})$ to ensure positiveness. For the two specific hyper-parameters of USNRT, we set the significance level $\alpha = 0.01$, and the minimum sample size in leaf nodes $N_{\text{min}} = \max\{N_{\text{train}}/10, 1000\}$, where N_{train} is the sample size of training data. This means that the constructed USNRT will have 10 leaf nodes at most, and about 3 levels (depth).

B. Competing Models

We compare USNRT to some recent popular models, including deep learning-based ones and traditional tree-based ones. They are Heteroskedastic Neural Network (HNN), Deep Ensemble, MC Dropout, Concrete Dropout, Extra Trees, and

Random Forest. They all produce means and variances for quantifying uncertainty, as USNRT does.

HNN and Deep Ensemble. In HNN, we build two neural networks to output the mean and the variance respectively. We train them alternately twice with negative log-likelihood loss, as suggested in [10]. Both the two networks have hidden layer sizes $[8d, 4d]$, with ReLU and Tanh activations respectively. The output layer activations are linear and Softplus respectively. Deep Ensemble [9] trains 5 such HNNs with different random initialization seeds. The five means and variances are aggregated to obtain one mean and one variance to finally quantify uncertainty.

Bayesian Approximations. MC Dropout [6] and Concrete Dropout [7] are popular Bayesian approximation models recently. In our experiment, MC Dropout has hidden layer sizes $[8d, 16d, 4d]$, dropout rate 0.5, ReLU/linear as hidden/output layer activation, and mean square error as loss function. Concrete Dropout has hidden layer sizes $[8d, 4d]$ and the dropout rate can be learned in the model (the official code released is used). After training, both the two models generate 1,000 predictions under the dropout mode for computing the mean and the variance.

Tree Models. We also compare USNRT to two tree-based models which can output both the mean and the variance, the Extremely Randomized Trees (ExTra) [24] and the Random Forests [23]. We select their hyper-parameters with the negative log-likelihood loss on the validation set. The number of trees is in the range $\{50, 100, 150, 200\}$, the tree depth is in $\{4, 6, 8, 10, 12\}$, and the proportion of features used for node splitting is in $\{0.3, 0.5, 0.7, 0.9\}$. We use the implements in the scikit-optimize package [29].

It is notable that among all competing methods, Deep Ensemble is the most computationally costly because 5 HNNs need to be trained. Even for training one HNN, the computational cost is higher than or close to that of training an USNRT. Because the cost of training an HNN is equivalent to that of training four ordinary neural networks with the same size, while in USNRT, it is about three or at most four in our setting.

C. Evaluation Metrics

Given a testing dataset $\{(\mathbf{X}(i), \mathbf{y}(i))\}_{i \in \mathcal{I}_{te}}$, for any method that can output the mean and the variance for $\mathbf{y}(i)$ given $\mathbf{X}(i)$, we use three evaluation metrics to evaluate it. They are expected calibration error (ECE), tail-interval calibration error (TCE), and sharpness. Denoting the mean and the variance given by the method as $\tilde{\mu}_i$ and $\tilde{\sigma}_i^2$, we first compute the predicted conditional τ_k -quantile of $\mathbf{y}(i)$ given $\mathbf{X}(i)$ under the Gaussian assumption:

$$\hat{q}_{i,k} = \tilde{\mu}_i + \tilde{\sigma}_i \Phi^{-1}(\tau_k), \quad (8)$$

where $\Phi^{-1}(\cdot)$ is the inverse of the distribution function of standard Gaussian. We choose $\tau_k \in \Pi = \{0.01, 0.02, \dots, 0.99\}$, where $k = 1, \dots, 99$. With these predicted quantiles, we introduce the evaluation metrics as follows.

1) *Expected Calibration Error (ECE)*: In the regression problem, calibration means that the probability that the observed random variable is lower than the τ -quantile equals the

expected probability τ . Here for τ_k , the observed probability is

$$\hat{P}_k^{\text{ece}} = \frac{1}{|\mathcal{I}_{te}|} \sum_{i \in \mathcal{I}_{te}} \mathbf{1}_{\{\mathbf{y}(i) < \hat{q}_{i,k}\}}. \quad (9)$$

It is ideal if $\hat{P}_k^{\text{ece}} = \tau_k$. Our ECE computes the difference between them and takes the average over all k :

$$\text{ECE} = 100 \times \frac{1}{K} \sum_{k=1}^K |\hat{P}_k^{\text{ece}} - \tau_k|. \quad (10)$$

The $K = 99$ probability levels in Π spread the interval $(0, 1)$, and hence ECE evaluates the full estimated distribution.

2) *Tail-Interval Calibration Error (TCE)*: In many uncertainty quantification works, the prediction intervals are required to be generated. The calibration of interval means that the probability that the observed random variable is located in the interval equals the expected probability, for example, 90%. Usually the predicted 5%- and 95%-quantiles are used to form the interval in this case. Now for $\tau_k < 0.5$, we construct the interval as $[\hat{q}_{i,k}, \hat{q}_{i,100-k}]$ and the observed probability is

$$\hat{P}_k^{\text{tce}} = \frac{1}{|\mathcal{I}_{te}|} \sum_{i \in \mathcal{I}_{te}} \mathbf{1}_{\{\hat{q}_{i,k} < \mathbf{y}(i) < \hat{q}_{i,100-k}\}}. \quad (11)$$

The corresponding expected probability is $1 - 2\tau_k$. Ideally, they are equal. Our TCE computes their difference and takes the average over some k :

$$\text{TCE} = 100 \times \frac{1}{|\Pi'|} \sum_{\tau_k \in \Pi'} |\hat{P}_k^{\text{tce}} - (1 - 2\tau_k)|, \quad (12)$$

where $\Pi' = \{0.05, 0.1, 0.15, 0.2\}$. This makes TCE the average calibration error of 90%, 80%, 70%, and 60% intervals.

3) *Sharpness*: When calibration is one side of evaluating uncertainty estimation, sharpness is another side to complement the evaluation. Supposing a model outputs $\tilde{\mu}_i, \tilde{\sigma}_i^2$ such that $\mathcal{N}(\tilde{\mu}_i, \tilde{\sigma}_i^2)$ is the unconditional distribution of $\{\mathbf{y}(i)\}_{i \in \mathcal{I}_{te}}$, we may obtain nearly perfect calibration although it's not what we want. Sharpness measures the length of the intervals constructed in TCE and makes narrow intervals preferred. One needs to find a good balance between calibration and sharpness. In our experiment, the quantiles are computed under the Gaussian assumption as in Equation (8). So, the length of the interval is proportional to the standard deviation $\tilde{\sigma}_i$. Instead, we can measure $\tilde{\sigma}_i$ directly in our sharpness metric:

$$\text{sharpness} = 100 \times \frac{1}{|\mathcal{I}_{te}|} \sum_{i \in \mathcal{I}_{te}} \tilde{\sigma}_i. \quad (13)$$

It is an alternative to the commonly-used interval sharpness $100 \times \frac{1}{|\mathcal{I}_{te}|} \sum_{i \in \mathcal{I}_{te}} |\hat{q}_{i,100-k} - \hat{q}_{i,k}|$ for any k because of Equation (8).

D. Comparison of Results

ECE. Table II shows ECE results of the seven methods on 17 datasets. As we can see, USNRT performs the best among all on 11 datasets out of 17, and performs the second best or above on 16 datasets out of 17. This is indeed a significantly superior performance. Moreover, on some datasets such as Conditional, Appliances, Real-time, Facebook1, Facebook2,

TABLE II: **ECE** results. The bold number represents the best performance, and the second best is marked by *. USNRT wins the best among all on 11 datasets out of 17, and wins the second best or above on 16 datasets out of 17. The last column shows the percentage decrease of USNRT’s result over the best of other six methods’. On datasets Conditional, Appliances, Real-time, Facebook1, Facebook2, and Wave, the percentage decrease is close to or larger than 50%.

Dataset \ Method	HNN	Deep Ensemble	MC Dropout	Concrete Dropout	Extra Trees	Random Forest	USNRT	Percentage Decrease
Electrical	*2.91	7.31	8.40	3.19	9.38	6.09	2.29	21.2%
Conditional	*3.50	7.55	20.84	8.53	15.80	11.49	1.37	61.0%
Appliances	*9.22	11.77	23.26	10.84	14.68	13.87	5.16	44.0%
Real-time	*12.84	13.60	23.00	17.07	23.11	22.90	3.01	76.6%
Industry	*4.65	11.76	17.76	9.36	8.87	11.53	4.56	1.9%
Facebook1	*9.98	14.27	26.82	16.37	14.33	12.23	4.86	51.3%
Beijing	3.42	4.76	11.82	4.92	7.28	6.04	*3.77	-10.1%
Physicochemical	2.65	4.41	15.10	3.82	5.51	6.03	*2.79	-5.4%
Traffic	3.75	3.78	21.54	3.76	3.45	*3.51	3.64	-5.7%
Blog	13.76	18.66	27.42	*13.50	17.79	17.02	12.18	9.8%
Power	2.11	1.76	16.28	2.14	2.53	2.09	*2.07	-17.8%
Online	*1.86	7.37	12.45	4.71	6.41	5.87	1.77	5.0%
Facebook2	*10.84	14.88	22.80	15.22	14.67	12.61	4.97	54.1%
Year	3.56	4.42	21.14	24.85	7.63	7.05	*4.16	-16.7%
Query	*1.40	5.34	11.73	2.68	12.24	9.56	1.24	11.8%
GPU	3.04	5.33	19.95	6.57	8.17	5.95	*3.14	-3.5%
Wave	12.55	18.87	15.71	10.76	9.45	*5.98	1.79	70.1%

TABLE III: **TCE** results. The bold number represents the best performance, and the second best is marked by *. USNRT wins the best among all on 10 datasets out of 17, and wins the second best or above on 16 datasets out of 17. The last column shows the percentage decrease of USNRT’s result over the best of other six methods’. On datasets Appliances, Real-time, Facebook1, Beijing, Facebook2, Year, and Wave, the percentage decrease is close to or larger than 50%.

Dataset \ Method	HNN	Deep Ensemble	MC Dropout	Concrete Dropout	Extra Trees	Random Forest	USNRT	Percentage Decrease
Electrical	6.77	14.48	13.97	2.35	19.33	14.18	*4.69	-99.0%
Conditional	1.46	15.64	62.67	13.79	24.47	20.50	*1.80	-23.7%
Appliances	*12.12	16.77	34.01	14.97	19.25	18.76	5.71	52.9%
Real-time	*12.92	23.21	13.01	19.96	24.11	23.71	5.32	58.8%
Industry	3.80	22.79	23.05	17.10	20.14	20.71	*6.81	-79.1%
Facebook1	14.51	19.99	*14.10	22.72	18.78	15.29	6.84	51.5%
Beijing	*4.13	8.48	30.66	5.58	11.77	8.86	1.74	58.0%
Physicochemical	2.25	6.91	41.99	3.50	10.09	10.87	*2.44	-8.5%
Traffic	7.61	7.75	64.92	7.56	6.62	*6.89	7.13	-7.7%
Blog	*17.72	21.88	19.48	19.89	21.46	20.63	14.23	19.7%
Power	2.26	2.78	48.30	*2.22	7.06	6.66	2.06	7.0%
Online	*2.47	16.17	7.42	7.01	14.54	12.84	2.34	5.4%
Facebook2	15.80	20.40	*13.71	19.59	20.04	17.24	8.06	41.2%
Year	*4.35	6.76	58.44	25.00	10.95	9.90	2.11	51.4%
Query	1.03	13.45	17.51	4.09	22.36	19.21	*1.80	-76.0%
GPU	2.61	14.76	25.70	4.82	17.65	13.75	*3.57	-37.0%
Wave	20.51	24.84	24.96	21.42	18.98	*14.24	2.24	84.3%

and Wave, the improvement of USNRT’s result over the others’ best is close to or larger than 50% (the last column). Overall, the second-place winner is HNN, which also performs quite well. Unfortunately, MC Dropout does not give reasonable calibration results.

TCE. Table III shows TCE results on 17 datasets. As we can see, USNRT performs the best among all on 10 datasets out of 17, and performs the second best or above on 16 datasets out of 17. This performance is excellent, considering the difficulty of tail-side calibration. Moreover, on datasets Appliances, Real-time, Facebook1, Beijing, Facebook2, Year, and Wave, the improvement of USNRT’s result over the others’ best is close to or larger than 50%. Overall, the second-place winner is again HNN. Relatively, all the remaining methods give unsatisfactory TCE results.

Sharpness. Table IV shows sharpness results on 17 datasets.

We can find that MC Dropout gives extremely small sharpness while Concrete Dropout gives extremely large sharpness sometimes. These two methods are unstable or cannot achieve a good balance between calibration and sharpness. If excluding MC Dropout, USNRT performs the best on 6 datasets out of 17, and the second best or above on 10 datasets out of 17, indicating that USNRT is doing well on both calibration and sharpness (on calibration, it is excellent). Besides, HNN and Random Forest give acceptable performance on sharpness.

E. Stability Analysis

In this subsection, we show that USNRT’s performance is stable with respect to the changing hyper-parameters. The structure of neural networks in internal nodes and the structure in leaf nodes are of course important hyper-parameters. Besides, USNRT has two additional hyper-parameters used

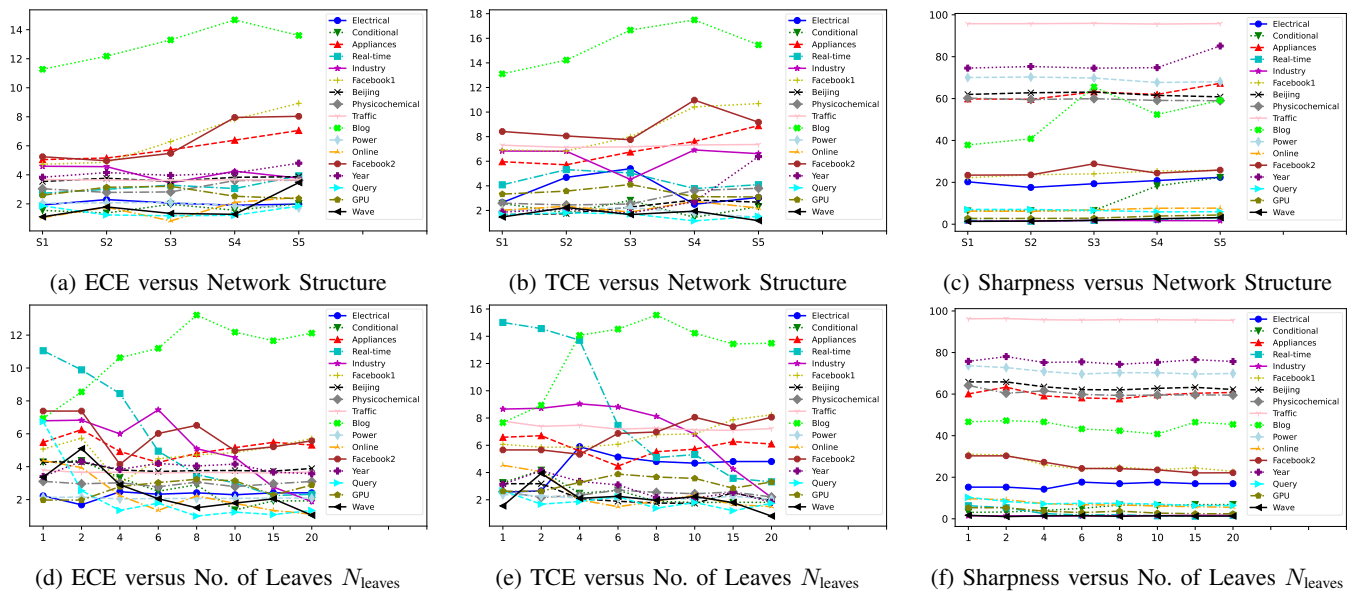


Fig. 1: The performance versus varying hyper-parameters on every dataset. (a)–(c): five different network structure combinations are in the x -axis, and from S1 to S5, the networks become larger and larger. One can find small networks are good enough for producing good ECE and TCE results. (d)–(f): the maximum number of leaf nodes N_{leaves} varies in $\{1, 2, 4, 6, 8, 10, 15, 20\}$ in the x -axis. On some datasets such as Conditional, Real-time, Industry, Online, Query, and Wave, ECE and TCE decrease substantially as N_{leaves} increases. On other datasets except Blog, ECE and TCE decrease moderately or remain stable.

TABLE IV: **Sharpness** results. The bold number represents the best performance, and the second best is marked by *. If excluding MC Dropout (no balance between calibration and sharpness), USNRT performs the best on 6 datasets out of 17, and the second best or above on 10 datasets out of 17.

Dataset	HNN	Deep Ensemble	MC Dropout	Concrete Dropout	Extra Trees	Random Forest	USNRT
Electrical	11.56	14.06	41.71	*12.82	58.81	48.42	17.57
Conditional	3.34	*3.76	16.57	799766	37.06	24.36	6.41
Appliances	67.32	71.65	28.83	78.53	75.59	72.23	*59.62
Real-time	2.92	3.42	27.63	–	1.81	*1.74	1.41
Industry	1.29	1.77	28.90	3.06	6.82	4.09	*1.50
Facebook1	26.87	33.64	28.16	–	*21.96	18.03	23.62
Beijing	63.95	66.61	33.82	68.21	74.93	67.41	*62.77
Physicochemical	60.59	63.83	32.63	42594	79.79	67.73	*59.54
Traffic	96.57	96.55	12.17	53832	95.94	*95.04	95.76
Blog	47.26	60.49	35.39	–	*27.46	24.81	40.80
Power	71.75	73.69	24.31	74.95	79.00	*69.37	70.28
Online	6.12	7.23	42.65	26.00	12.54	9.38	*6.17
Facebook2	32.47	38.38	32.91	–	*21.45	17.83	23.55
Year	*74.35	75.17	16.36	–	90.95	86.08	75.31
Query	*7.59	8.84	38.60	17.85	21.76	10.97	7.05
GPU	3.69	4.51	26.63	10.51	4.97	*3.40	2.74
Wave	0.01	*0.01	25.62	6.05	4.73	4.07	1.47

in seeking the best split: the significance level α and the minimum sample size in leaf nodes N_{min} . Generally, α can be set to 0.01 without change, as in usual statistical tests. So, we will not analyze it in the following.

For neural network structures, we change the hidden layers and consider five different combinations of the two structures in internal nodes and leaf nodes: $[4d, 2d] + [4d, 2d]$, $[8d, 4d] + [4d, 2d]$, $[16d, 8d] + [8d, 4d]$, $[8d, 16d, 4d] + [4d, 8d, 2d]$, and $[16d, 16d, 8d] + [8d, 8d, 4d]$. They make the networks more and more complex. We implement USNRT with them and plot the corresponding varying performance using the three metrics, as shown in Figure 1 (a)–(c), where each line corresponds to a dataset. One can see that larger networks do not neces-

sarily lead to better ECE or TCE. Indeed, $[4d, 2d] + [4d, 2d]$ or $[8d, 4d] + [4d, 2d]$ (S1, S2 in the horizontal axis) is enough for good performance, and they have lower computational costs. The sharpness results are quite stable with respect to the changing structures. Conclusively, there is no need to carefully pick neural network structures.

Similarly, we study the effect of the minimum sample size in leaf nodes N_{min} on the performance. For better illustration, we define $N_{min} = \max\{N_{train}/N_{leaves}, 1000\}$, where N_{train} is the size of training dataset, and N_{leaves} will be the number of leaf nodes at most. We change N_{leaves} in $\{1, 2, 4, 6, 8, 10, 15, 20\}$ and plot the corresponding varying performance in Figure 1 (d)–(f). We can find that on some datasets such as Conditional, Real-time, Industry, Online, Query, and Wave, ECE and TCE results decrease substantially as N_{leaves} increases. On other datasets except Blog, ECE and TCE decrease moderately or remain stable. This may be because different datasets have different degrees of heterogeneity. The sharpness results are quite stable again. So, setting N_{leaves} to 8 or 10 will be an appropriate choice in moderation, and has acceptable computational cost as well.

VI. VISUALIZATION AND INTERPRETATION

A. Probability-Wise Interval Calibration

In Equation (12), we define TCE as the average of four interval calibration errors. Now we elaborate it by computing probability-wise interval calibration error

$$C_k = 100 \times |\hat{P}_k^{tce} - (1 - 2\tau_k)|, \quad (14)$$

for all k such that $1 - 2\tau_k \in \{0.1, 0.2, \dots, 0.9\}$ (i.e., the expected probability is 0.1, 0.2, \dots , 0.9). For each method in the

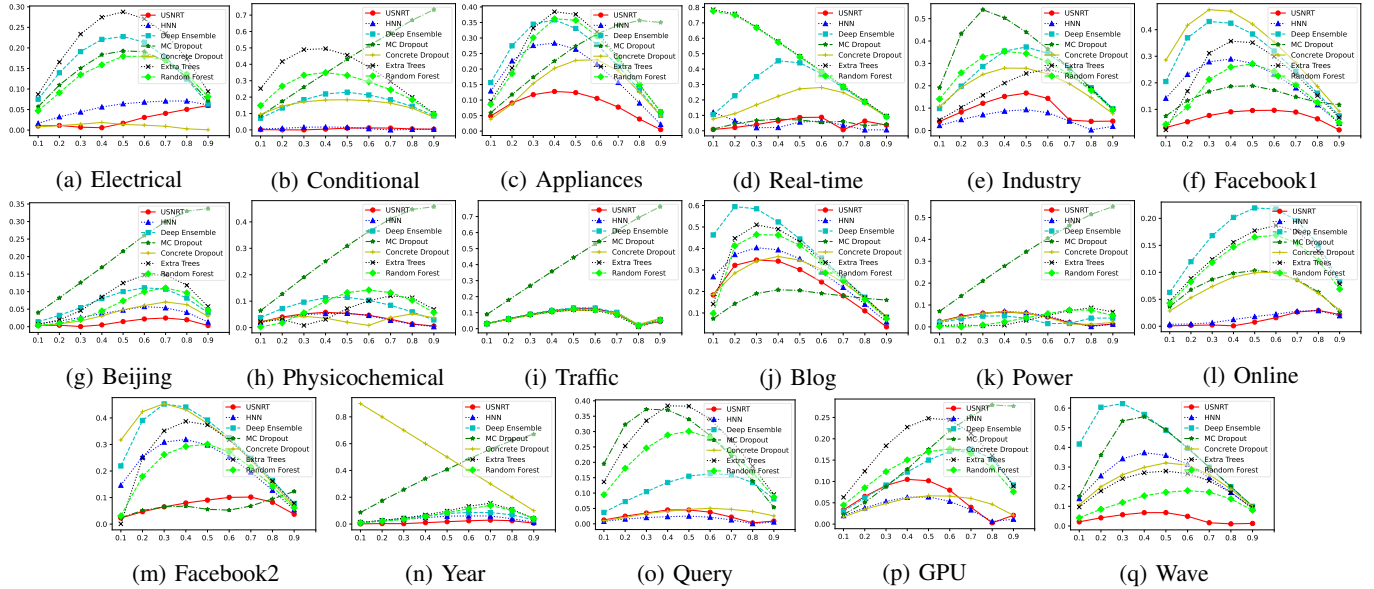


Fig. 2: Visualization of probability-wise interval calibration for 17 UCI datasets. The horizontal axis is the expected probability and the vertical axis is the calibration error. Different lines represent different methods, and the red one is USNRT. The closer the line is to 0, the better. USNRT’s line is always in a low position. On most datasets, it performs the best or the second best.

experiment, we plot these probability-wise calibration errors (averaged over the multiple training/testing splits) against the varying expected probability from 0.1 to 0.9, in Figure 2. Each dataset corresponds to one subfigure, and different lines with distinct colors and markers represent different methods. The red ones with circles are given by USNRT. The closer the line is to 0, the better the performance. As we can see, in every subfigure, USNRT’s line keeps in a low position, indicating that USNRT is capable of providing well-calibrated intervals for distinct expected probability levels or coverage rates. Actually, in most subfigures, USNRT performs the best or the second best among all methods.

B. Space Partitioning at Root Node

Here we visualize how USNRT partitions the feature space, taking the partitioning at the first node or root node as an example. At the root node, USNRT partitions the whole space into two regions. Figure 3 shows the results on 6 datasets: Electrical, Appliances, Facebook1, Physicochemical, Year, and Wave (under one specific training/testing split). The whole feature space is projected to two-dimensional using the split variable and one of other variables. The squared residuals $(\mathbf{y}(i) - \hat{f}_{\text{split}}(\mathbf{X}(i)))^2$ for all i are plotted as scattering points with different color depths. The color depths represent the scales of squared residuals after a quantile transformation (to uniform distribution). The dashed line gives the best partition found by USNRT. We also compute the left-region residuals’ variance and the right-region residuals’ variance (before the quantile transformation) to form a legend. One can find that the left and right variances are significantly different, indicating the possibility of distinct uncertainty natures. The color depths also illustrate such a difference. Such partitioning will be

done recursively by USNRT until no heterogeneity can be discovered anymore under some criteria.

C. Uncertainty Heterogeneity across Leaf Regions

On each dataset, after learning an USNRT (under one specific training/testing split), we compute the leaf region-specific residuals’ variance using all $(\mathbf{y}(i) - \hat{f}_m(\mathbf{X}(i)))^2$ when $\mathbf{X}(i) \in \mathcal{R}_m$. After obtaining the variances, we then compute the standard deviations and plot them as scattering points in Figure 4. Each marker corresponds to one dataset. We can see that in many cases, those standard deviations of leaf regions in one dataset are significantly different or heterogeneous, sometimes spreading from 0 to 1. This indicates that separate leaf regions have distinct uncertainty natures. Some exceptive datasets include Real-time, Industry, GPU, and Wave. This partially reveals the reason of USNRT’s success and the difficulty of quantifying uncertainty using one model for the whole feature space. USNRT treats the leaf regions separately after obtaining those leaf regions by tree-structured learning. We can also conclude that the uncertainty heterogeneity widely exists in real-world data.

VII. MORE RELATED WORKS

A. Mixture Models and Other Tree Models

Our work shares some similarities with Hierarchical Mixture of Experts (HMEs) [30] in a small extent. HMEs are soft local-regression models which adopt multiple local models and combine them in a probabilistic way, like Mixture of Gaussians for clustering. Generally, EM algorithm needs to be used to learn the parameters of such probabilistic models. This may be computationally inefficient when neural networks are used as local models. While we use the hard-splitting tree structure, it will be more natural to incorporate neural networks.

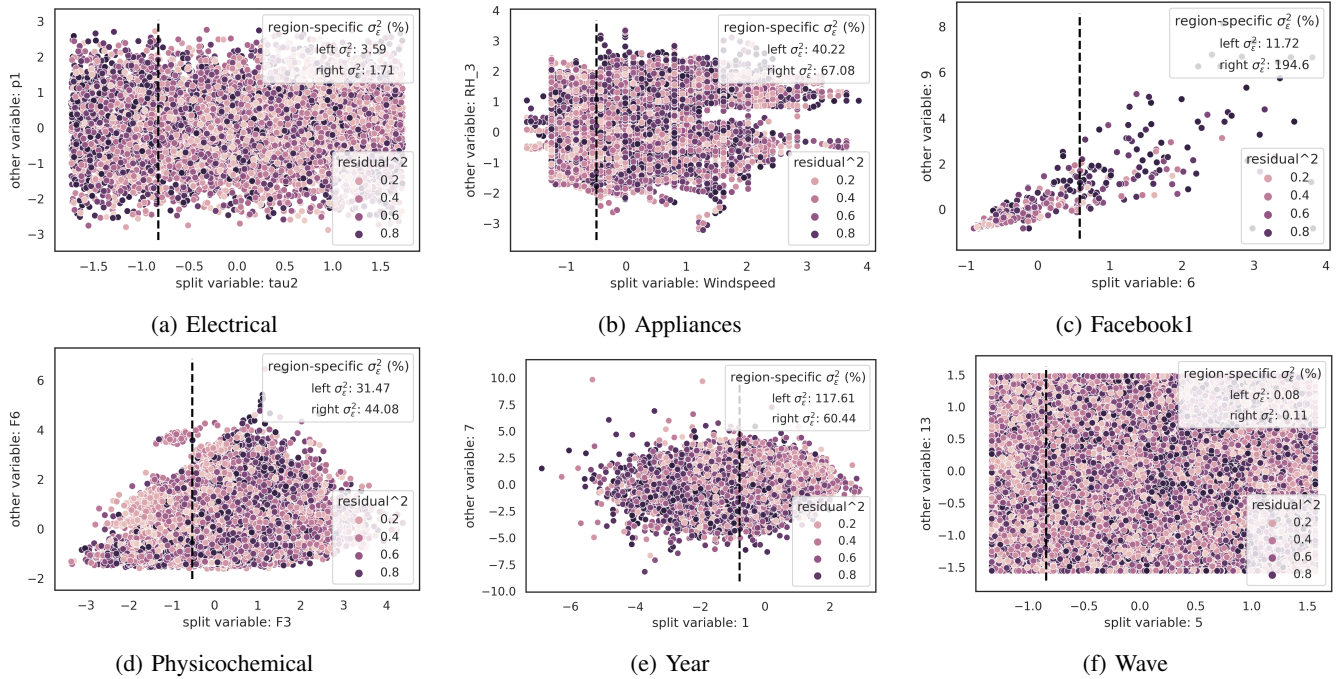


Fig. 3: Visualization of the partitioning at root node for six datasets: Electrical, Appliances, Facebook1, Physicochemical, Year, and Wave. The whole feature space is projected to two-dimensional. The squared residuals after fitting \hat{f}_{split} are plotted with different color depths (after a quantile transformation). The dashed line gives the best partition found by USNRT. One can find that the left-region residuals’ variance and the right-region residuals’ variance are significantly different, especially in datasets Electrical, Facebook1, and Year.

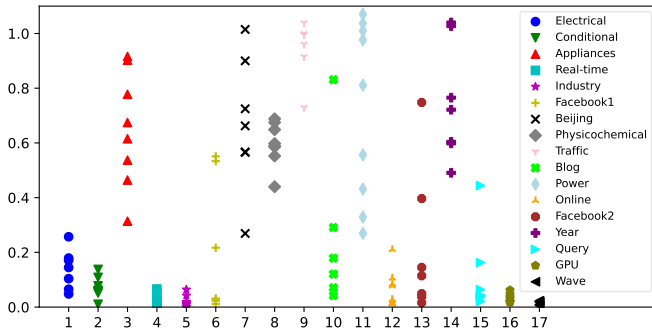


Fig. 4: Leaf region-specific residuals’ standard deviations of USNRT. Each type of marker corresponds to one dataset. In many cases, those standard deviations of one dataset are significantly different or heterogeneous, sometimes spreading from 0 to 1. This indicates that separate leaf regions have distinct uncertainty natures.

Tree models are a big family. Chi-Square Automatic Interaction Detector (CHAID) proposed by [31] determines the best multiway splits by conducting statistical tests too. However, CHAID is preferred when there are many categorical variables and is more suitable for target selection problems. The representatives of other ensemble tree models include Gradient Boosting Decision Tree (GBDT) [32] and LightGBM [33]. They are both boosting-type and generally do not output a variance for the prediction.

B. Other Methods for Uncertainty Quantification

Except for variance-based methods (the main focus of this paper) for uncertainty quantification in regression, there are still other types of methods such as quantile-based interval constructions and new loss functions designed for predicting the whole distribution.

Estimating quantiles does not need any parametric assumptions on the distribution. Two symmetric quantiles (about probability 0.5) can form the prediction interval we need. Vanilla quantile regression [34], [35] has a long history in statistics and econometrics, and pinball loss is the core of the literature. Recently in machine learning, [13] proposed Simultaneous Quantile Regression (SQR) which models the quantile function (inverse of CDF) as a partial neural network and can estimate all the conditional quantiles of the label simultaneously. [36] proposed orthogonal quantile regression which utilizes the independence between the interval length and the indicator of miscoverage to design a new regularization term. [15] proposed several new loss functions or training procedures to overcome the shortcomings of pinball loss and obtained intervals with better calibration and sharpness results. [14] proposed a novel conformalized quantile regression with the advantages of both conformal prediction and quantile regression, which aims to construct prediction intervals that can achieve finite sample calibration.

Besides, some new loss functions have been proposed to estimate the whole conditional distribution for quantifying uncertainty. [12] used Maximum Mean Discrepancy as a distribution matching strategy to construct calibrated regression.

[37] proposed Collaborating Networks which use two distinct networks to represent the quantile function and its inverse (CDF), and proposed novel loss functions to learn them as well. [38] estimated heterogeneous conditional distributions by combining uncountable asymmetric Laplacians.

C. Aleatory Uncertainty and Epistemic Uncertainty

The source of uncertainty can be generally categorized into two kinds, epistemic uncertainty and aleatory uncertainty [39]. Epistemic uncertainty or systematic uncertainty is caused by a lack of knowledge, and can be reduced by increasing additional information [38], [40]. For example, one can add prior information to the model through the Bayesian approach [4]–[8], [41]–[43], or expanding the training data.

Aleatory uncertainty or statistical uncertainty refers to randomness which cannot be reduced by any additional information. This type of uncertainty can be quantified by outputting the full conditional distribution, rather than the point-wise prediction. Many popular methods are proposed to estimate the aleatory uncertainty, such as variance networks [10], quantile regressions [14], [15], [36], conformal predictions [14], [44], [45], and distribution predictions [37]. Our method also belongs to this kind.

VIII. CONCLUSION

In this paper, we propose a tree-structured local learning model USNRT to recursively partition the feature space and improve uncertainty quantification of variance networks. It is motivated by the widely-existing data heterogeneity in real-world datasets. With the help of a statistical test, we design a splitting procedure to discover the uncertainty heterogeneity across regions in the feature space and construct the tree. Region-specific neural networks are employed to output both the mean and the variance. USNRT has acceptable computational cost and pruning is unnecessary. Experiments on extensive UCI datasets demonstrate that USNRT outperforms some recent popular models. Through visualization, we also show that USNRT can indeed discover uncertainty heterogeneity in the datasets. Moreover, USNRT's performance is stable with respect to the varying neural network structures. It is also easy to determine the most important hyper-parameter: the minimum sample size in leaf nodes (or equivalently, maximum number of leaf nodes).

In the future, it is necessary to take data heterogeneity into consideration for building up better machine learning models, through the techniques of data partitioning like in this paper. It is also interesting to see other forms of combination of deep learning and tree models, although this paper only focuses on uncertainty quantification.

APPENDIX

A. THE PROOF OF PROPOSITION 3

Proof: Without loss of generality, we assume f_0 and f_1 are discontinuous at the point x^* on the boundary between \mathcal{D}_0 and \mathcal{D}_1 . In the case where σ_0 and σ_1 are discontinuous, the proof is similar. Suppose $\min_{f \in \mathcal{F}, \sigma \in \mathcal{F}'} \mathbb{E}[l(\mathbf{y}, f(\mathbf{X}), \sigma(\mathbf{X}))]$

is solved at f^*, σ^* , because f^* is a continuous function and f_0, f_1 are continuous on $\overline{\mathcal{D}_0}$ and $\overline{\mathcal{D}_1}$ respectively, we can find a hypercube H centered at x^* with length δ such that:

$$\begin{aligned} |f^*(x) - f^*(x^*)| &< \epsilon/8, & x \in H, \\ |f_0(x) - f_0(x^*)| &< \epsilon/8, & x \in H \cap \mathcal{D}_0, \\ |f_1(x) - f_1(x^*)| &< \epsilon/8, & x \in H \cap \mathcal{D}_1, \end{aligned}$$

where $\epsilon = |f_1(x^*) - f_0(x^*)|$. Because $\epsilon \leq |f_1(x^*) - f^*(x^*)| + |f^*(x^*) - f_0(x^*)|$, we have $|f_1(x^*) - f^*(x^*)| \geq \epsilon/2$, or, $|f^*(x^*) - f_0(x^*)| \geq \epsilon/2$. Without loss of generality, we assume the latter is true, then

$$\begin{aligned} \epsilon/2 &\leq |f^*(x^*) - f_0(x^*)| \leq \\ &|f^*(x^*) - f^*(x)| + |f^*(x) - f_0(x)| + |f_0(x) - f_0(x^*)| \\ &< \epsilon/8 + |f^*(x) - f_0(x)| + \epsilon/8, \quad \text{when } x \in H \cap \mathcal{D}_0. \end{aligned}$$

So $|f^*(x) - f_0(x)| > \epsilon/4$ for all $x \in H \cap \mathcal{D}_0$. This further implies $f^*(x) - f_0(x) > \epsilon/4$, $\forall x \in H \cap \mathcal{D}_0$, or, $f^*(x) - f_0(x) < -\epsilon/4$, $\forall x \in H \cap \mathcal{D}_0$. No matter which one is true, we can always successfully construct an $f_2 \in \mathcal{F}$ according to the condition 3), such that $f_2(x) = 0$ when $x \notin H$ and $0 > f_2(x) > -\epsilon/4$ (or $0 < f_2(x) < \epsilon/4$) when $x \in H$. Then

$$\begin{aligned} f^*(x) &> (f^* + f_2)(x) > f_0(x), & x \in H \cap \mathcal{D}_0, \\ (f^* + f_2)(x) &= f^*(x), & x \in H^c \cap \mathcal{D}_0. \end{aligned}$$

The new function $f^* + f_2$ gives:

$$\begin{aligned} &\mathbb{E}[l(\mathbf{y}_0, (f^* + f_2)(\mathbf{X}_0), \sigma^*(\mathbf{X}_0))] \\ &< \mathbb{E}[l(\mathbf{y}_0, f^*(\mathbf{X}_0), \sigma^*(\mathbf{X}_0))]. \end{aligned}$$

This inequality holds because \mathbf{X}_0 and \mathbf{X}_1 have positive densities around x^* and l is a proper loss such that a better $f \in \mathcal{F}$ will lead to a smaller expected risk. With this inequality, we have

$$\begin{aligned} &\mathbb{E}[l(\mathbf{y}, f^*(\mathbf{X}), \sigma^*(\mathbf{X}))] \\ &= \mathbb{E}[\mathbb{E}[l(\mathbf{y}, f^*(\mathbf{X}), \sigma^*(\mathbf{X})) | Z]] \\ &= (1-p)\mathbb{E}[l(\mathbf{y}_0, f^*(\mathbf{X}_0), \sigma^*(\mathbf{X}_0))] \\ &\quad + p\mathbb{E}[l(\mathbf{y}_1, f^*(\mathbf{X}_1), \sigma^*(\mathbf{X}_1))] \\ &> (1-p)\mathbb{E}[l(\mathbf{y}_0, (f^* + f_2)(\mathbf{X}_0), \sigma^*(\mathbf{X}_0))] \\ &\quad + p\mathbb{E}[l(\mathbf{y}_1, f^*(\mathbf{X}_1), \sigma^*(\mathbf{X}_1))] \\ &\geq (1-p) \min_{f \in \mathcal{F}, \sigma \in \mathcal{F}'} \mathbb{E}[l(\mathbf{y}_0, f(\mathbf{X}_0), \sigma(\mathbf{X}_0))] \\ &\quad + p \min_{f \in \mathcal{F}, \sigma \in \mathcal{F}'} \mathbb{E}[l(\mathbf{y}_1, f(\mathbf{X}_1), \sigma(\mathbf{X}_1))]. \end{aligned}$$

Here we can finish the proof. ■

REFERENCES

- [1] Y. LeCun, Y. Bengio, and G. Hinton, "Deep learning," *nature*, vol. 521, no. 7553, pp. 436–444, 2015.
- [2] C. Guo, G. Pleiss, Y. Sun, and K. Q. Weinberger, "On calibration of modern neural networks," in *International Conference on Machine Learning*. PMLR, 2017, pp. 1321–1330.
- [3] R. Rahaman *et al.*, "Uncertainty quantification and deep ensembles," *Advances in Neural Information Processing Systems*, vol. 34, 2021.

- [4] C. Blundell, J. Cornebise, K. Kavukcuoglu, and D. Wierstra, "Weight uncertainty in neural network," in *International conference on machine learning*. PMLR, 2015, pp. 1613–1622.
- [5] J. M. Hernández-Lobato and R. Adams, "Probabilistic backpropagation for scalable learning of bayesian neural networks," in *International conference on machine learning*. PMLR, 2015, pp. 1861–1869.
- [6] Y. Gal and Z. Ghahramani, "Dropout as a bayesian approximation: Representing model uncertainty in deep learning," in *international conference on machine learning*. PMLR, 2016, pp. 1050–1059.
- [7] Y. Gal, J. Hron, and A. Kendall, "Concrete dropout," *Advances in neural information processing systems*, vol. 30, 2017.
- [8] W. J. Maddox, P. Izmailov, T. Garipov, D. P. Vetrov, and A. G. Wilson, "A simple baseline for bayesian uncertainty in deep learning," *Advances in Neural Information Processing Systems*, vol. 32, 2019.
- [9] B. Lakshminarayanan, A. Pritzel, and C. Blundell, "Simple and scalable predictive uncertainty estimation using deep ensembles," *Advances in neural information processing systems*, vol. 30, 2017.
- [10] N. Skafte, M. Jørgensen, and S. Hauberg, "Reliable training and estimation of variance networks," *Advances in Neural Information Processing Systems*, vol. 32, 2019.
- [11] S. Zhao, T. Ma, and S. Ermon, "Individual calibration with randomized forecasting," in *International Conference on Machine Learning*. PMLR, 2020, pp. 11 387–11 397.
- [12] P. Cui, W. Hu, and J. Zhu, "Calibrated reliable regression using maximum mean discrepancy," *Advances in Neural Information Processing Systems*, vol. 33, pp. 17 164–17 175, 2020.
- [13] N. Tagasovska and D. Lopez-Paz, "Single-model uncertainties for deep learning," *Advances in Neural Information Processing Systems*, vol. 32, 2019.
- [14] Y. Romano, E. Patterson, and E. Candes, "Conformalized quantile regression," *Advances in neural information processing systems*, vol. 32, 2019.
- [15] Y. Chung, W. Neiswanger, I. Char, and J. Schneider, "Beyond pinball loss: Quantile methods for calibrated uncertainty quantification," *Advances in Neural Information Processing Systems*, vol. 34, 2021.
- [16] X. Fan, B. Li, and S. Sisson, "Rectangular bounding process," *Advances in Neural Information Processing Systems*, vol. 31, 2018.
- [17] S. Ge, S. Wang, Y. W. Teh, L. Wang, and L. Elliott, "Random tessellation forests," *Advances in Neural Information Processing Systems*, vol. 32, 2019.
- [18] J. H. Friedman, "Multivariate adaptive regression splines," *The annals of statistics*, vol. 19, no. 1, pp. 1–67, 1991.
- [19] J. Wang and V. Saligrama, "Local supervised learning through space partitioning," *Advances in Neural Information Processing Systems*, vol. 25, 2012.
- [20] H. Oiwa and R. Fujimaki, "Partition-wise linear models," *Advances in Neural Information Processing Systems*, vol. 27, 2014.
- [21] P. Chaudhuri, M.-C. Huang, W.-Y. Loh, and R. Yao, "Piecewise-polynomial regression trees," *Statistica Sinica*, pp. 143–167, 1994.
- [22] X. Zheng and S. X. Chen, "Partitioning structure learning for segmented linear regression trees," *Advances in Neural Information Processing Systems*, vol. 32, 2019.
- [23] L. Breiman, "Random forests," *Machine learning*, vol. 45, no. 1, pp. 5–32, 2001.
- [24] P. Geurts, D. Ernst, and L. Wehenkel, "Extremely randomized trees," *Machine learning*, vol. 63, no. 1, pp. 3–42, 2006.
- [25] L. Breiman, J. H. Friedman, R. A. Olshen, and C. J. Stone, *Classification and regression trees*. Routledge, 2017.
- [26] H. Levene, "Robust tests for equality of variances," *Contributions to probability and statistics. Essays in honor of Harold Hotelling*, pp. 279–292, 1961.
- [27] D. Dua and C. Graff, "UCI machine learning repository," 2017. [Online]. Available: <http://archive.ics.uci.edu/ml>
- [28] D. P. Kingma and J. Ba, "Adam: A method for stochastic optimization," in *International Conference on Learning Representations*, 2015.
- [29] scikit-optimize. [Online]. Available: <https://scikit-optimize.github.io/stable/>
- [30] M. I. Jordan and R. A. Jacobs, "Hierarchical mixtures of experts and the em algorithm," *Neural computation*, vol. 6, no. 2, pp. 181–214, 1994.
- [31] G. V. Kass, "An exploratory technique for investigating large quantities of categorical data," *Journal of the Royal Statistical Society: Series C (Applied Statistics)*, vol. 29, no. 2, pp. 119–127, 1980.
- [32] J. H. Friedman, "Greedy function approximation: a gradient boosting machine," *Annals of statistics*, pp. 1189–1232, 2001.
- [33] G. Ke, Q. Meng, T. Finley, T. Wang, W. Chen, W. Ma, Q. Ye, and T.-Y. Liu, "Lightgbm: A highly efficient gradient boosting decision tree," *Advances in neural information processing systems*, vol. 30, 2017.
- [34] R. Koenker and G. Bassett Jr, "Regression quantiles," *Econometrica: journal of the Econometric Society*, pp. 33–50, 1978.
- [35] R. Koenker and K. F. Hallock, "Quantile regression," *Journal of economic perspectives*, vol. 15, no. 4, pp. 143–156, 2001.
- [36] S. Feldman, S. Bates, and Y. Romano, "Improving conditional coverage via orthogonal quantile regression," *Advances in Neural Information Processing Systems*, vol. 34, pp. 2060–2071, 2021.
- [37] T. Zhou, Y. Li, Y. Wu, and D. Carlson, "Estimating uncertainty intervals from collaborating networks," *Journal of Machine Learning Research*, vol. 22, no. 257, pp. 1–47, 2021.
- [38] A. Brando, J. A. Rodriguez, J. Vitria, and A. Rubio Muñoz, "Modelling heterogeneous distributions with an uncountable mixture of asymmetric laplacians," *Advances in neural information processing systems*, vol. 32, 2019.
- [39] A. Der Kiureghian and O. Ditlevsen, "Aleatory or epistemic? does it matter?" *Structural safety*, vol. 31, no. 2, pp. 105–112, 2009.
- [40] E. Hüllermeier and W. Waegeman, "Aleatoric and epistemic uncertainty in machine learning: An introduction to concepts and methods," *Machine Learning*, vol. 110, no. 3, pp. 457–506, 2021.
- [41] A. Graves, "Practical variational inference for neural networks," *Advances in neural information processing systems*, vol. 24, 2011.
- [42] Y. Li, J. M. Hernández-Lobato, and R. E. Turner, "Stochastic expectation propagation," *Advances in neural information processing systems*, vol. 28, 2015.
- [43] D. P. Kingma, T. Salimans, and M. Welling, "Variational dropout and the local reparameterization trick," *Advances in neural information processing systems*, vol. 28, 2015.
- [44] G. Shafer and V. Vovk, "A tutorial on conformal prediction," *Journal of Machine Learning Research*, vol. 9, no. 3, 2008.
- [45] H. Papadopoulos, V. Vovk, and A. Gammerman, "Regression conformal prediction with nearest neighbours," *Journal of Artificial Intelligence Research*, vol. 40, pp. 815–840, 2011.